Development of a macro-element model for rockfall steel wires using Experimental and Numerical data

Previtali, Marco; Ciantia, Matteo; Spadea, Saverio; Castellanza, Riccardo; Crosta, Giovanni

Published in:
Proceedings of the 18th UK Travelling Workshop

DOI:
10.20933/100001232

Publication date:
2021

Development of a macro-element model for rockfall steel wires using Experimental and Numerical data

Marco Previtali[1]*, Matteo Ciantia[1], Saverio Spadea[1], Riccardo Castellanza[2], Giovanni Crosta[2]

[1] School of Science and Engineering, University of Dundee, Dundee, UK.

[2] Department of Earth and Environmental Sciences, University of Milano-Bicocca, Milan, Italy.

*m.previtali@dundee.ac.uk

Key words: *Tensile testing; Macro-element; Rockfall protection; Multiscale analysis*

Abstract

This paper aims to present a few aspects of the development of a plastic-hardening macro-element model for steel wires in flexible protection systems. First, the material behaviour is obtained using uniaxial tensile tests. Successively, the evolution of the elastic and plastic domain is obtained using a combination of physical tests, analytical models, and numerical simulations. Finally, the results obtained with the macro-element model are compared to those obtained using other approaches found in literature.

Introduction

In recent years, the numerical simulation of passive structures for the mitigation of rockfall hazard has received significant attention. This is due to the advances in computational power, that allow for higher complexity, and in remote sensing, that drive the need for more accurate models (Salvini *et al.*, 2017; Mentani *et al.*, 2018). In this context, the majority of models adopt a multi-scale approach, in which the local-scale element response (i.e. wires, interweavements) is reproduced at the mesh scale using an equivalent numerical object (i.e. truss beam) (Nicot *et al.*, 2001). However, the numerical objects adopted typically make use of very simplistic constitutive models, meaning they require strong assumptions, limiting their applicability. The "macro-element" approach uses a constitutive model to reproduce the local-scale behaviour at the meso-scale, expressing the system state through generalized stress-strain variables (i.e. force and displacement). Since their introduction (Nova and Montrasio, 1991), they became a popular practice in geotechnical engineering for their simplicity, efficiency and accuracy (NOVA and PARMA, 2011; Dattola *et al.*, 2016). Herein a macro-element model is developed to provide a more accurate local-scale response for interweaved double-twisted meshes using an isotropic plastic hardening model with associated flow rule. Finally, results of a numerical punching test obtained from the experimental force-displacement curve and the macro-element are compared.

Model definition

The wire behaviour is elastic inside a subspace of the generalized stress space, i.e. force and moment $\boldsymbol{q}$, defined by the Yield Surface f. In this area, the relationship between stress and strain is linear, following classic beam theory. When the stress state reaches the yield surface, successive strain increments are absorbed through plastic deformation. Since the model adopted is isotropic hardening, the yield surface expands according to the hardening function $\boldsymbol{\alpha}$, which depends on a set of history variables, herein defined as the generalized strains $\boldsymbol{\delta_{pl}}$. The entity of these deformations, the plastic multiplier γ, is obtained from the Prager's consistency condition (Prager, 1949), so that the yield surface expansion is equal to the generalized stress increments.

$$\gamma f(\boldsymbol{q}, \boldsymbol{\alpha}) = 0 \quad (1)$$

$$\partial f = \frac{df}{d\boldsymbol{q}}\dot{\boldsymbol{q}} + \frac{df}{d\boldsymbol{\alpha}}\dot{\boldsymbol{\alpha}} \tag{2}$$

$$\dot{\boldsymbol{\alpha}} = \frac{d\boldsymbol{\alpha}}{d\boldsymbol{\delta}_{pl}}\dot{\boldsymbol{\delta}_{pl}} \tag{3}$$

Finally, the plastic multiplier is split between the two generalized plastic strains depending on the plastic potential g:

$$\dot{\boldsymbol{\delta}_{pl}} = \frac{dg}{d\boldsymbol{q}}\gamma \tag{4}$$

Herein, an associated plasticity model is adopted, meaning $g = f$.

Experimental setup

The material behaviour is characterized using uniaxial tensile tests. The wire (60 mm long, 2.7 mm thick) is clamped between two wedge grips and loaded under strain-controlled conditions (2 mm / min). The deformation values registered by the instrument are not reliable as the wire slides through the wedges. Rather than increasing the grip, which can cause localized failure, the effective displacement is obtained using an extensometer. Unfortunately, the deformation of the double-twisted interweavements cannot be measured in this fashion due to their non-flat surface, which causes the extensometer to detach from the wire after some displacement. Therefore, image analysis has been employed to measure the double-twisted strain, after calibrating it on the single-wire extensometer results (Figure 1). The grayscale image is first binarized using an adaptive gray-level histogram threshold (Otsu, 1979). Then, the wire region is extracted using 8-connected-component labelling (Vincent *et al.*, 1991). The wire length and width are obtained from the normalized second central moments of the region (Rizon *et al.*, 2006). The same instrument has been used to carry out three-point bending tests.

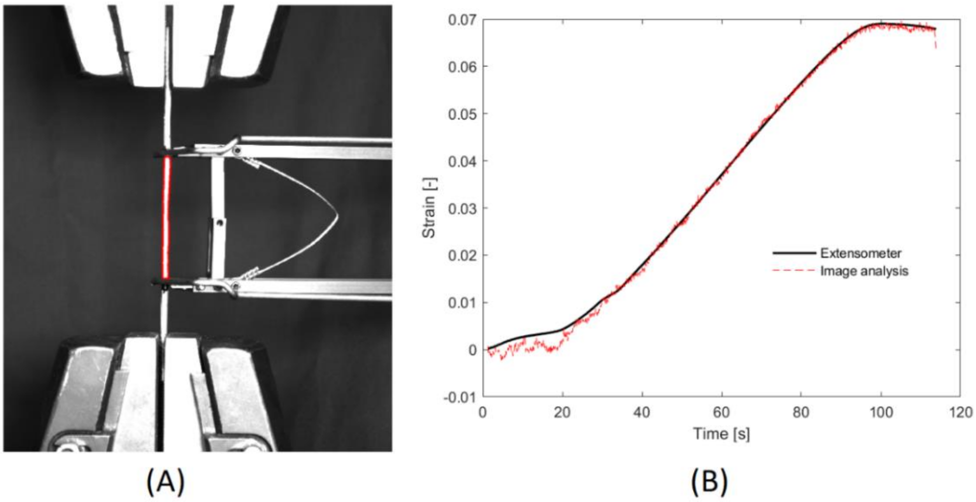

Figure 1: (a) wire distortion measured using an extensometer and (b) comparison of the strain data provided through image analysis and extensometer.

Surface calibration

For single-wires, the yield surface is obtained using classic beam theory. The wire cross section is split into slices and the fiber strain within each is obtained from the contributions of total wire strain ε and curvature χ.

$$\varepsilon_{slice} = \varepsilon_{wire} + \chi_{wire} \cdot b_{slice} \tag{5}$$

Where b is the branch between a given slice and the neutral axis of the wire face. The stress state within the slice is then obtained from the experimental stress-strain curve. A set of radial loading paths is defined and the initial shape of the yield surface is obtained as the combination of force F and moment M that cause a steel fiber to undergo plasticization. The same is done for the ultimate surface, where all the fibers within the section area reach a plateau in the stress-strain curve. As the elastic model is perfectly linear, the shape of the initial yield surface in the F-M space is always a triangle, while the ultimate is a semi-circle (Di Laora *et al.*, 2020). For each strain increment, given the current stress state within a slice, it is possible to calculate the equivalent strain under pure elastic conditions. Follows that the plastic strain within each slice is obtained as the difference between the two. The overall plastic strain is then obtained as the sum of these components, while the angular plastic strain is the sum of the products of these and the slices branches. For the double-twists, the yield surface and plastic potential evolution has been obtained using a finite element model. The material behaviour is obtained from the single-wire tests. The wire geometry and loading conditions of the test are reproduced using symmetric master-slave contact interactions. Successively, a quasi-static tensile test is carried out and calibrated using the experimental double-twist pulling test dataset. A few equations have been tested to fit the surfaces, considering the necessity of (i) continuous derivatives within the parametric space, (ii) a local peak at $F = 0$ and (iii) axis orthogonal derivatives at the domain extremities. The equation proposed by (Leuthold *et al.*, 2021) fits the yield surface and plastic potential at both the initial and ultimate state. However, this approach has the drawback that it requires the calibration of three extra functions to describe the surface parameter evolution, which significantly limits the applicability of the model. For the purpose of calibration, it is easier to use two different surfaces for the initial and ultimate conditions, which are obtained analytically from the material yield stress and the wire geometry. Successively, the surface at a given step is obtained by interpolating between the two through a negative exponential function:

$$f(u_{pl}, \theta_{pl}) = f_{init} \mathrm{e}^{(\mathrm{k_n u_{pl}} + k_m \theta_{pl})} + f_{ult}\left(1 - \mathrm{e}^{(\mathrm{k_n u_{pl}} + k_m \theta_{pl})}\right) \tag{6}$$

Where k_n and k_m are fitting parameters (< 0), which are obtained directly from the uniaxial tensile and bending tests.

Numerical tests

The meso-scale behaviour of the macro-element is evaluated through semi-static punch tests. A semi-spherical platter, moving at a constant speed, is used to load to a 3x3m mesh panel, pinned at the edges. Reaction force is measured on the platter. Details are available in (Previtali *et al.*, 2020b). Test #1 and #2 use the standard experimental force-displacement curve approach (Previtali *et al.*, 2020a), the former with the tensile tester data, the latter the same data after the image analysis/extensometer correction. Finally Test #3 uses the macro-element model. As shown in Figure 2, for out-of-plane loads, the force-displacement relationship is more affected by the introduction of a bending moment at the contact interface than a change in contact stiffness under uniaxial conditions.

Conclusions

In this paper, a few experimental tests were carried out to calibrate a macro-element model. An image-analysis procedure is developed to remove the effect of wire and clamp slippage from the dataset. Successively, the procedure used to calibrate the yield surface and plastic potential is described. Due to the significant changes in the function shape, two surfaces are used instead: (i) initial linear yield surface and (ii) ultimate failure envelope. The effective plastic potential at any step is then obtained by using an interpolation function. Finally, the model response is evaluated against the classic uniaxial stress-strain curve approach using quasi-static punch tests. The results highlight the importance of moving past the uniaxial force-displacement curve approach.

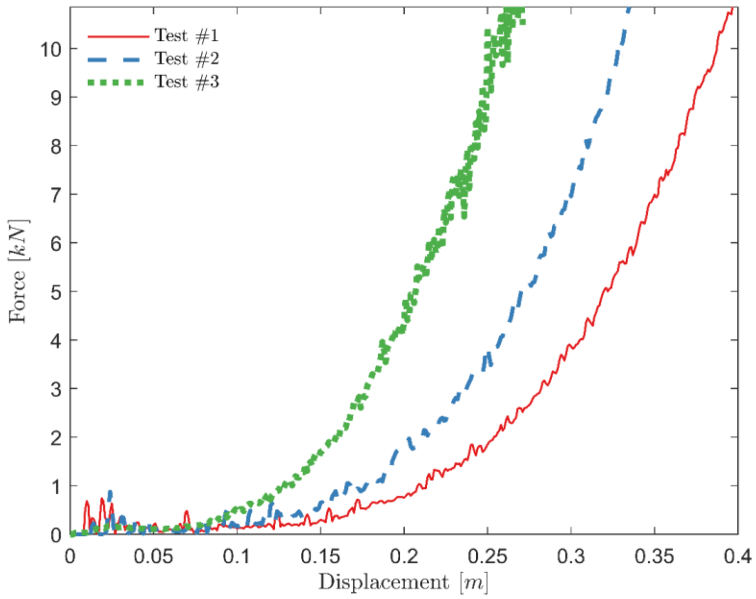

Figure 2: Force-displacement relationship acting on the platter

References

Dattola, G., Crosta, G. and Di Prisco, C. (2016) *Modelling boulder impacts on deformable layers: role of rolling and toppling*, *Geophysical Research Abstracts*.

Di Laora, R., Galasso, C., Mylonakis, G. and Cosenza, E. (2020) A simple method for *N-M* interaction diagrams of circular reinforced concrete cross sections, *Structural Concrete*. doi: 10.1002/suco.201900139.

Leuthold, J., Gerolymatou, E. and Triantafyllidis, T. (2021) Effect of Compaction Banding on the Hydraulic Properties of Porous Rock - Part II: Constitutive Description and Numerical Simulations, *Rock Mechanics and Rock Engineering*. Springer, 1, p. 3. doi: 10.1007/s00603-021-02430-1.

Mentani, A., Govoni, L., Giacomini, A., Gottardi, G. and Buzzi, O. (2018) An Equivalent Continuum Approach to Efficiently Model the Response of Steel Wire Meshes to Rockfall Impacts, *Rock Mechanics and Rock Engineering*. Springer Vienna, 51(9), pp. 2825–2838. doi: 10.1007/s00603-018-1490-5.

Nicot, F., Cambou, B. and Mazzoleni, G. (2001) Design of Rockfall Restraining Nets from a Discrete Element Modelling, *Rock Mechanics and Rock Engineering*. Springer-Verlag, 34(2), pp. 99–118. doi: 10.1007/s006030170017.

Nova, R. and Montrasio, L. (1991) Settlement of shallow foundations on sands.

NOVA, R. and PARMA, M. (2011) Effects of bond crushing on the settlements of shallow foundations on soft rocks, *Géotechnique*. Thomas Telford Ltd , 61(3), pp. 247–261. doi: 10.1680/geot.7.00183.

Otsu, N. (1979) THRESHOLD SELECTION METHOD FROM GRAY-LEVEL HISTOGRAMS., *IEEE Trans Syst Man Cybern*, SMC-9(1), pp. 62–66. doi: 10.1109/TSMC.1979.4310076.

Prager, W. (1949) Recent developments in the mathematical theory of plasticity, *Journal of Applied Physics*. American Institute of Physics, 20(3), pp. 235–241. doi: 10.1063/1.1698348.

Previtali, M., Ciantia, M., Castellanza, R. and Crosta, G. B. (2020a) Mesh sensitivity in discrete element simulation of flexible protection structures. Loughborough University. doi: 10.17028/rd.lboro.12102534.v1.

Previtali, M., Ciantia, M., Spadea, S., Castellanza, R. and Crosta, G. (2020b) Discrete element modeling of compound rockfall fence nets, in *IACMAG2020*, pp. 1–8.

Rizon, M., Haniza, Y., Puteh, S., Ali Yeon, M. S. P. D., Abdul Rahman, S., Mohd Rozailan, M., Sazali, Y. P. D., Hazri, D. D. and Karthigayan, M. (2006) Object detection using geometric invariant moment, *American Journal of Applied Sciences*. Science Publications, 2(6), pp. 1876–1878.

Salvini, R., Mastrorocco, G., Seddaiu, M., Rossi, D. and Vanneschi, C. (2017) The use of an unmanned aerial vehicle for fracture mapping within a marble quarry (Carrara, Italy): photogrammetry and discrete fracture network modelling, *Geomatics, Natural Hazards and Risk*. Taylor & Francis, 8(1), pp. 34–52. doi: 10.1080/19475705.2016.1199053.

Vincent, L., Vincent, L. and Soille, P. (1991) Watersheds in Digital Spaces: An Efficient Algorithm Based on Immersion Simulations, *IEEE Transactions on Pattern Analysis and Machine Intelligence*, 13(6), pp. 583–598. doi: 10.1109/34.87344.